PROCEEDINGS A

royalsocietypublishing.org/journal/rspa

Research

Cite this article: Lázaro JT, Alarcón T, Garay CP, Sardanyés J. 2023 Semiclassical theory predicts stochastic ghosts scaling. *Proc. R. Soc. A* **479**: 20220621.
https://doi.org/10.1098/rspa.2022.0621

Received: 22 September 2022
Accepted: 9 February 2023

Subject Areas:
applied mathematics, statistical physics, differential equations

Keywords:
complex systems, nonlinear stochastic dynamics, scaling laws, transients, universality

Authors for correspondence:
J. Tomás Lázaro
e-mail: jose.tomas.lazaro@upc.edu
Josep Sardanyés
e-mail: jsardanyes@crm.cat

Semiclassical theory predicts stochastic ghosts scaling

J. Tomás Lázaro[1,2,3,4], Tomás Alarcón[2,3,5,6], Carlos P. Garay[7,8] and Josep Sardanyés[2,3]

[1]Departament de Matemàtiques, Universitat Politècnica de Catalunya, Av. Diagonal 647, 08028 Barcelona, Spain
[2]Centre de Recerca Matemàtica (CRM), Campus de Bellaterra, Edifici C, 08193 Bellaterra, Barcelona, Spain
[3]Dynamical Systems and Computational Virology, CSIC Associated Unit CRM-I2SysBio, Spain
[4]Institute of Mathematics of the UPC-BarcelonaTech (IMTech), C. Pau Gargallo 14, 08028 Barcelona, Spain
[5]Pg. Lluís Companys 23, 08010 Barcelona, Spain
[6]Departament de Matemàtiques, Universitat Autònoma de Barcelona, 08193 Bellaterra, Barcelona, Spain
[7]Laboratorio Subterráneo de Canfranc, 22880 Canfranc-Estación, Huesca, Spain
[8]Institute for Integrative Systems Biology (I2SysBio), CSIC-Universitat de València, 46980 Paterna, Spain

JTL, 0000-0003-4395-9708; TA, 0000-0002-8566-3676; CPG, 0000-0003-1282-2944; JS, 0000-0001-7225-5158

Slowing down occurs in dynamical systems close to bifurcations or phase transitions. The time length (τ) of ghost transients close to a saddle-node bifurcation in deterministic systems follows $\tau \sim |\epsilon - \epsilon_c|^{-1/2}$, ϵ being the bifurcation parameter and ϵ_c its critical value. Recently, we numerically investigated how intrinsic noise affected the deterministic picture, finding a more complicated scaling law. We here provide a theoretical basis for this new law with two models of cooperation using a Wentzel–Kramers–Brillouin asymptotic approximation of the Master Equation. A study of the phase space of the Hamiltonian derived from the Hamilton–Jacobi equation shows that the statistically significant orbits (paths) reproduce the scaling function observed in the stochastic simulations. The flight times tied to these orbits underpin the scaling law of the stochastic system, and the same properties should extend in a universal way to all stochastic

THE ROYAL SOCIETY PUBLISHING

systems whose associated Hamiltonian exhibits the same behaviour. Our approach allows to make useful theoretical predictions of transient times in stochastic systems close to a bifurcation.

royalsocietypublishing.org/journal/rspa Proc. R. Soc. A 479: 20220621

1. Introduction

Slowing down phenomena are ubiquitous in dynamical systems, both stochastic and deterministic, approaching a phase transition or a bifurcation. Both these terms refer to a qualitative change in the dynamical behaviour of the system as a parameter, referred to as a control or bifurcation parameter, reaches its critical value [1–3]. In the vicinity of bifurcation points, slowing down phenomena occur whereby the transients towards equilibrium become much longer than those experienced far away from the critical bifurcation point [3–9].

An specific example can be found in deterministic systems undergoing a tipping point given by a saddle-node (s-n) bifurcation. In this bifurcation, the equilibrium points collide and get annihilated, as the colliding equilibria move to the complex domain ($\mathbb{C}$) after crossing the bifurcation [3,10–13]. Recent research has explored the dynamical mechanisms taking place at the complex phase space (in general, in $\mathbb{C}^n$) causing such slowdown in transients [14]. These delays are usually referred to as *delayed transitions* or *ghosts* [3,5]. The term ghost alludes to the attracting remnant left by the s-n collision in the region of the phase space where it occurs. This collision produces a bottleneck which hugely delays the dynamics in the deterministic system for suitable initial conditions.

S-n bifurcations typically arise in biological dynamical systems with strong nonlinearities such as cooperation (both intra- or interspecific) [9,11,12,14–16]. For instance, intra-specific cooperation is found in several species including social insects [17,18], marine species [19], bats [17] and primates [20]. Other self-cooperative processes are found in yeast [21] and in cancer cells via the autocrine signalling [22].

A remarkable property of slowing down behaviour close to critical points is that it is characterized by universal scaling laws [3–7]. For the deterministic s-n bifurcation, the scaling behaviour manifests in the form of a power law of the transient time τ towards the stable equilibrium (in many cases, the origin). Specifically, $\tau \sim |\epsilon - \epsilon_c|^{-1/2}$ holds, where ϵ is the control parameter and ϵ_c its critical value [3,12,23]. Such scaling power law and ghosts arising after s-n bifurcations have been identified in mathematical models of charge density waves [5], hypercycles [13,16] and ecological systems with facilitation including semi-arid ecosystems [15] and metapopulations with [10] and without [11,12] habitat destruction. Remarkably, this scaling law has been clearly identified experimentally in an electronic circuit [24].

Ghosts have been thoroughly analysed in deterministic systems [3,5,12–16,24–27]. However, recent computational studies have addressed the effects of intrinsic noise, i.e. fluctuations due to small population sizes, on the ghost phenomenon [13,15,16]. In a recent paper [28], we investigated, by means of extensive numerical simulations, the effects of such intrinsic noise on delayed transitions by using a simple model for autocatalysis and a two-member hypercycle. Somewhat contrary to intuition, we found that the ghost phenomenon was robust to intrinsic noise. Indeed, we showed that in stochastic systems close to a first-order phase transition, the relaxation dynamics toward the (unique) absorbing state experienced a slowing down but, being the system stochastic, the transient times showed variability in length for different realizations. Hence, we quantified the length of these transients by using the average extinction times $\bar{T}_e$ (see [28] for details). Extensive computational analysis of $\bar{T}_e$ performed with Gillespie simulations (GS) allowed us to ascertain that it exhibited a scaling behaviour. While the extinction time in deterministic systems close to the s-n bifurcation exhibits a simple power law scaling, $\bar{T}_e$ right after the stochastic bifurcation follows a more complex scaling behaviour of the form

$$\bar{T}_e \sim \Omega^{-b}\, \mathcal{G}(\Omega^a(\epsilon - \epsilon_c^{(s)})), \tag{1.1}$$

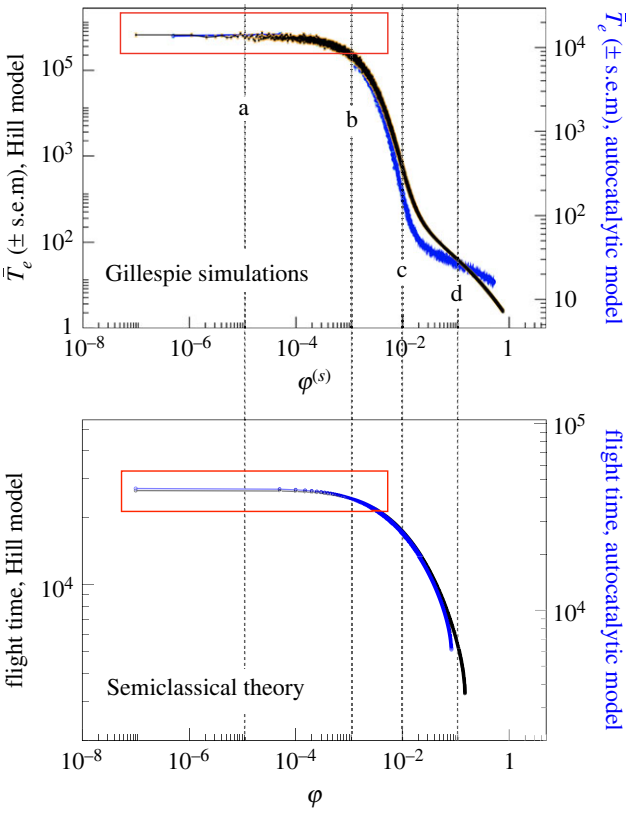

Figure 1. (Top) Scaling of the mean extinction times $\bar{T}_e(\pm\text{s.e.m})$ (computed averaging over 10^3 independent realizations) obtained from Gillespie simulations (GS), shown overlapped for the Hill (black data) and the autocatalytic (blue data) models using $x(0) = 0.75 \cdot \Omega$. Here, $\varphi^{(s)} = \epsilon - \bar{\epsilon}_c^{(s)}$ is the distance between the bifurcation parameter, ϵ, and the mean stochastic bifurcation value, $\bar{\epsilon}_c^{(s)}$. Close to the stochastic bifurcation transients' scaling remains flat (red rectangle). (Bottom) Scaling obtained for the flight times computed from the Hamiltonian system, averaging over 20 different initial conditions (variances are not shown for the sake of clarity) within the region of lowest action. In all of the analyses we used $\Omega = 10^3$. We show different representative dynamical regimes in terms of $\varphi = \epsilon - \epsilon_c$: (a) longer transients for $\varphi = 10^{-5}$, (b) bending of the flat scaling region at $\varphi \approx 10^{-3}$ and shorter transients with (c) $\varphi = 10^{-2}$ and (d) $\varphi = 10^{-1}$. The time scales of the GS (a) and flight times of the Hamiltonian system (b) appeared different (not shown here) due to the rescaling of the transition rates, equation (2.2). Such rescaling implies that the time scales associated with the Hamilton–Jacobi equation, equation (2.3), are smaller by a factor Ω with respect to that of the Master Equation, equation (2.1). In the lower panel, we show the values of the flight times multiplied by a factor Ω. (Online version in colour.)

where Ω is the system's size, ϵ and $\epsilon_c^{(s)}$ are the control parameter and its critical value in the stochastic system (with $\epsilon \gtrsim \epsilon_c^{(s)}$), respectively, a and b are scaling exponents and $\mathcal{G}(\cdot)$ the scaling function. The form of the scaling function $\mathcal{G}$ (numerically obtained) is shown in the upper panel of figure 1 (see also [28]). It is clear that the scaling behaviour of the stochastic ghosts is very different from that exhibited by their deterministic counterparts given by $\tau \sim |\epsilon - \epsilon_c|^{-1/2}$.

The investigation and our knowledge on scaling phenomena at the vicinity of bifurcations related to transient times has been largely developed in dynamical systems without stochasticity. Hence, the impact of intrinsic (multiplicative) noise in such scalings is currently poorly understood. In this sense, a theory explaining the shape of the scaling function $\mathcal{G}$ numerically identified in [28] is currently lacking. The aim of the work is to advance in this issue by providing a theoretical framework to better understand the changes introduced by intrinsic noise in delayed transitions phenomena. To do that, we address this problem by using the so-called

semiclassical approximation. This approach was first introduced as a Wentzel–Kramers–Brillouin (WKB) perturbative scheme in quantum mechanics to study the behaviour of the solutions of the Schrödinger equation. Its name is due to the fact that the WKB analysis of the Schrödinger yields the conclusion that the main features of the behaviour of the quantum-mechanical wave function are contributed by the classical Hamiltonian, or, more specifically by the classical action [29]. It is also closely related to the corresponding path integral formulation [30,31]. When applied to Markov-jump processes (MJPs) of the type we consider here and also in [28], we exploit the well-established analogy between the master equation (ME), i.e. the equation that dictates the dynamics of the MJPs, and the Schrödinger equation [31]. Within this context, the WKB method provides a solution of the ME in the limit $\Omega \gg 1$. This solution, as per the WKB method [32], is determined by the action linked to the trajectories associated with an *effective* Hamiltonian [30,32–37].

As mentioned, the aim of our contribution is to provide a theoretical (dynamical) approach explaining the origins of the scaling law caused by ghosts in stochastic s-n bifurcations. As we will show, our mathematical approach provides a dynamical basis explaining the impact of intrinsic noise in scaling phenomena at the vicinity of a tipping point with a discontinuity in the order parameter (such as in first-order phase transitions) as occurs in s-n bifurcations. The theory developed in this manuscript allows useful and accurate predictions of transient times just after stochastic bifurcations by determining the key properties of the Hamiltonian explaining the shape of the scaling law compared with its deterministic counterpart. The article is organized as follows. In §2, we summarize the theoretical framework used to analyse the stochastic dynamics. Sections 3 and 4 provide a detailed account of our results and their discussion, respectively.

2. Theoretical framework

In this section, we summarize how intrinsic noise is introduced in the general context of nonlinear birth-and-death processes. Assuming that the underlying stochastic dynamics is described by a Markovian process, the basic description of the process is given by the corresponding ME

$$\frac{\partial}{\partial t}P(X,t) = \sum_{r_i=\pm 1} (W_i(X - r_i)P(X - r_i) - W_i(X)P(X)), \tag{2.1}$$

where $X(t)$ is the state variable which corresponds to the number of individuals at time t, $P(X,t)$ is the probability density that the system has X individuals at time t, and the transition rates W_i and the stoichiometric coefficients r_i are such that

$$\text{Prob}(X(t + \Delta t) = X + r_i | X(t) = X) = W_i(X)\Delta t + \mathcal{O}(\Delta t^2).$$

In order to proceed further with our analysis, we assume that the transition rates, upon rescaling, satisfy the following scaling relation:

$$W_i(X) = \Omega w_i(x) + \mathcal{O}(\Omega^0), \tag{2.2}$$

where Ω is the system's size and $x = X/\Omega$ is the rescaled state variable. Note that rates derived from Law of Mass Action kinetics and Michaelis–Menten–Hill kinetics satisfy such conditions. If the transition rates satisfy equation (2.2), we can propose a WKB Ansatz for $P(X,t)$:

$$P(X,t) = \exp(-\Omega(S(x,t) + \mathcal{O}(\Omega^{-1}))),$$

which, when introduced in equation (2.1), at the lowest order, i.e. at $\mathcal{O}(\Omega^0)$, the function $S(x,t)$, the so-called action, satisfies the equation

$$\frac{\partial S}{\partial t} = H\left(x, \frac{\partial S}{\partial x}\right), \tag{2.3}$$

where the function $H(x,p)$ is given by

$$H(x,p) = \sum_{r_i=\pm 1} (\mathrm{e}^{r_i p} - 1) w_i(x), \tag{2.4}$$

p being the Hamiltonian conjugate momentum of x. The action also maps the stochastic process to a path integral representation [31], formalism that can be studied using tools developed in equilibrium statistical physics. The path integral replaces the deterministic unique trajectory by a functional integral over an infinity of stochastic possible trajectories. Hence, this integral provides a mapping U_t between probability generating functions at different times and a field theory in the continuum limit.

The transition probability of a trajectory Γ connecting the point x_i (at time t_i) with the point x_f (at time t_f) in phase space, can be written as

$$P(x_f, t_f | x_i, t_i) = \int_\Gamma \mathrm{d}x\, \mathrm{d}p\, \mathrm{e}^{-\Omega \int (p\dot{x} - H(x,p))\, \mathrm{d}t}, \tag{2.5}$$

where the Hamiltonian $H(x,p)$ determines the motion of a *particle* moving on Γ. Recall that the action tied to the path Γ is given by

$$S(\Gamma) = \int_\Gamma (p\dot{x} - H(x,p))\, \mathrm{d}t,$$

which plays the role of probability measure—weighted by the system size Ω—in equation (2.5). All these possible trajectories Γ are weighted by the action S, which satisfies a Hamilton–Jacobi equation (like (2.3)) with Hamiltonian, in this case, given by (2.4). Altogether suggests a classical mechanical interpretation where the trajectories of such a particle are given by the solutions of the associated Hamilton's equations:

$$\left.\begin{aligned} \dot{x} &= \frac{\partial H}{\partial p} = \sum_{r_i=\pm 1} r_i \mathrm{e}^{r_i p} w_i(x), \\ \dot{p} &= -\frac{\partial H}{\partial x} = -\sum_{r_i=\pm 1} (\mathrm{e}^{r_i p} - 1) \frac{\mathrm{d}w_i}{\mathrm{d}x}. \end{aligned}\right\} \tag{2.6}$$

The Hamiltonian formulation of the stochastic processes given by equation (2.6) has been used to study problems as the quasi-steady state distribution in connection with first passage problems [32–37], the statistics of rare events in reaction–diffusion systems [30], and the path integral representation of the process [31], among others. Here, we use the Hamiltonian formulation, specifically the structure of the corresponding phase space, to determine which of its generic features lend robustness of the ghost with intrinsic noise thus causing long transients as it happens with the mean-field ghosts. We further investigate how the scaling form of the relaxation time is an emergent property of such generic features showing that this mathematical formulation allows for useful predictions of the transient times of the stochastic system.

3. Results

Using the theoretical framework discussed in the previous section, we are ready to explore stochastic systems whose mean-field limit undergoes a s-n bifurcation. Our goal is to explain the numerically observed robustness of the ghost to intrinsic noise and the scaling of the mean extinction times, $\bar{T}_e$, in the autocatalytic (i.e. intra-specific cooperation) replicator model, given by

$$\dot{x} = k\, x^2 (1 - x) - \epsilon\, x, \tag{3.1}$$

$k > 0$ being the intrinsic growth rate and $\epsilon > 0$ the decay rate (see [28] for the stochastic numerical results and [10,12,16] for further information on the dynamics of this model). For completeness and consistency of results, we also analyse the Hill model [38] with linear decay, which exhibits

Table 1. Transition rates for the two specific model examples investigated in this paper: the autocatalytic model [28] and the Hill system [38], both including growth, different saturation functions (i.e. logistic and cooperative Hill) and exponential decay.

model system	transition rates	stoichiometry coefficient	description
autocatalyic	$W_1 = k_1 X$	$r_1 = +1$	birth
autocatalyic	$W_2 = (k_1/C\Omega^2)X(X-1)(X-2)$	$r_2 = -1$	competition for finite resources
autocatalyic	$W_3 = \epsilon X$	$r_3 = -1$	death
Hill	$W_1 = \Omega(k_1 X^2/(\Omega^2 A^2 + X^2))$	$r_1 = +1$	birth with saturation
Hill	$W_2 = \epsilon X$	$r_2 = -1$	death

the same mean-field bifurcation. This model is given by

$$\dot{x} = \frac{k\,x^2}{A^2 + x^2} - \epsilon\, x. \tag{3.2}$$

Here, $k > 0$ and $\epsilon > 0$ are synthesis and degradation rates, $A > 0$ being a saturation constant. We anticipate that the behaviour of these two models is similar near the bifurcation and thus our results will be presented alternating both systems. Stochastic simulations will be carried out using Gillespie simulations (hereafter labeled as GS) [39,40]. Together with the GS algorithms, we will use the seventh-eighth order Runge–Kutta–Fehlberg–Simó method for numerical integration of the differential equations (software available in [41]).

We have first computed the scaling of the mean extinction times $\bar{T}_e$ with GS, for the two models considered (see table 1 and [28] for the procedure used to compute these extinction times). Briefly said, $\bar{T}_e$ have been computed by averaging the extinction times over 10^3 realizations of the GS for values of ϵ close to beyond the stochastic bifurcation. The stochastic bifurcation point has been computed using a fine numerical tuning of ϵ, increasing its values and choosing the first value involving extinctions in 10^3 realizations of the GS (setting time to 10^8 and $x(0) = 0.75 \cdot \Omega$). The bifurcation value has been chosen as the average of 50 independent replicas of the previous process and is given with precision of seven decimal positions, obtaining $\bar{\epsilon}_c^{(s)}$. Specifically, we have studied how $\bar{T}_e$ changes as $\varphi^{(s)} = \epsilon - \bar{\epsilon}_c^{(s)}$ varies. That is, the control parameter is driven beyond this mean stochastic bifurcation value obtained numerically. From the results, the first observation is that, close to the bifurcation, the behaviour of both models is characterized by the same scaling function (see the upper panel in figure 1). Second, far from the stochastic bifurcation value the scaling behaviour is lost, and $\bar{T}_e$ shows model-specific features, as expected.

We will show that the scaling obtained with the GS is well captured by the semiclassical theory, based on the dynamics' study of the Hamiltonian systems (2.6). It is important to highlight that both models share a similar phase space structure, which clearly determines their dynamics. Let us present them, separately.

Let us consider first the *Hill model*. According to table 1, one has $r_1 = +1$, $r_2 = -1$ and

$$W_1(X) = \Omega\,\frac{k_1 X^2}{\Omega^2 A^2 + X^2}, \quad W_2(X) = \epsilon X.$$

Taking $x = X/\Omega$, it follows that

$$w_1(x) = \frac{W_1(x\Omega)}{\Omega} = \frac{k_1 x^2}{A^2 + x^2} \quad \text{and} \quad w_2(x) = \frac{W_2(x\Omega)}{\Omega} = \epsilon x,$$

and, therefore, the Hamiltonian function (2.4) becomes

$$H(x,p) = (\mathrm{e}^p - 1)w_1(x) + (\mathrm{e}^{-p} - 1)w_2(x) = (\mathrm{e}^p - 1)\frac{k_1 x^2}{A^2 + x^2} + (\mathrm{e}^{-p} - 1)\epsilon x.$$

Without loss of generality, we can take $k_1 = 1$. Now, if we perform the change of variables in space $(x,p) \mapsto (y = \frac{x}{A}, p)$, in time $t = A\sigma$, redefine the parameter $\epsilon \to A\epsilon$, and denote again $y = x$

and $\sigma = t$, the corresponding Hamiltonian system (2.6) takes the form

$$\left.\begin{aligned} \dot{x} &= \mathrm{e}^{p}\frac{x^2}{1+x^2} - \mathrm{e}^{-p}\epsilon x, \\ \dot{p} &= -(\mathrm{e}^{p}-1)\frac{2x}{(1+x^2)^2} - (\mathrm{e}^{-p}-1)\epsilon, \end{aligned}\right\} \tag{3.3}$$

with associated Hamiltonian function

$$H(x,p) = \frac{x^2}{1+x^2}(\mathrm{e}^{p}-1) + \epsilon x(\mathrm{e}^{p}-1).$$

The deterministic limit (3.2), obtained for $p = 0$, has three equilibrium points: $x = 0$ (attracting) and $x_{\pm} = (1/2\epsilon)(1 \pm \sqrt{1-4\epsilon^2})$, x_- being a repeller and x_+ an attractor. The s-n bifurcation occurs at $\epsilon = \epsilon_{\mathrm{c}} = 1/2$, at which $x_{\pm}$ collide in a non-trivial critical equilibrium point $x_{\mathrm{crit}} = 1/2\epsilon_{\mathrm{c}} = 1$. For $\epsilon \geq \epsilon_{\mathrm{c}}$ (or, equivalently, $\varphi = \epsilon - \epsilon_{\mathrm{c}} \geq 0$), its dynamics is driven by the following curves (figures 2 and 3):

— The solution of $H(x,p) = 0$, which is formed by three curves, namely: $x = 0$, $p = 0$, and $p = p_H(x)$, where

$$p_H(x) := \log\left(\epsilon\,\frac{1+x^2}{x}\right).$$

Note that $p_H(x) = 0$ only intersects the axis $p = 0$ when $\epsilon = \epsilon_{\mathrm{c}}$. Precisely, $p = p_H(x)$ goes to $+\infty$ as $x \to 0^+$ and as $x \to +\infty$, and it has a unique global minimum, at $x_{\mathrm{min,\,H}} = 1$, with value $p_{\mathrm{min,\,H}} = p_H(x_{\mathrm{min,\,H}}) = \log 2\epsilon$.

— The x-nullcline $\dot{x} = 0$, formed by the curves $x = 0$ and $p = p_1(x) := (1/2)p_H(x)$, with a global minimum at $x_{\mathrm{min,\,H}}$ and $p_1(x_{\mathrm{min,\,H}}) = (1/2)\log(2\epsilon)$.

— The p-nullcline $\dot{p} = 0$, given in two components: $p = 0$ and $p = p_2(x)$, where

$$p_2(x) := \log\left(\frac{\epsilon(1+x^2)^2}{2x}\right) = p_H(x) + \log\left(\frac{1+x^2}{2}\right).$$

It has a global minimum at $x_{\mathrm{min,\,p}} = 1/\sqrt{3}$ with value $p_{\mathrm{min,\,p}} = p_2(x_{\mathrm{min,\,p}}) = \log((8\sqrt{3}/9)\epsilon)$. This curve $p = p_2(x)$ intersects $p = 0$ at two points, $x_F(\epsilon) \leq x_0(\epsilon)$, moves upwards as ϵ increases and becomes tangent for $\epsilon = \epsilon_{\mathrm{end}} = 3(\sqrt{3}/8) \simeq 0.649519053$. In other words, for $\varphi \simeq 4 \times 10^{-1}$. It is inside the region determined by the curve $\dot{p} = 0$, the invariant axis $p = 0$ (a component of $H = 0$) and $p < 0$ where the trajectories of our system exhibit the scaling behaviour shown in figure 1 (lower panel).

An analogue situation holds for the *autocatalytic model*, where one has $w_1(x) = k_1 x^2$ and $w_2(x) = k_1 x^3 + \epsilon x$. As before, we take $k_1 = 1$. The Hamiltonian function becomes

$$H(x,p) = x^2(\mathrm{e}^{p}-1) + (x^3+\epsilon x)(\mathrm{e}^{-p}-1),$$

and leads to the system

$$\left.\begin{aligned} \dot{x} &= x^2\mathrm{e}^{p} - (x^3+\epsilon x)\mathrm{e}^{-p}, \\ \dot{p} &= -2x(\mathrm{e}^{p}-1) - (3x^2+\epsilon)(\mathrm{e}^{-p}-1). \end{aligned}\right\} \tag{3.4}$$

Hence, the relevant curves are

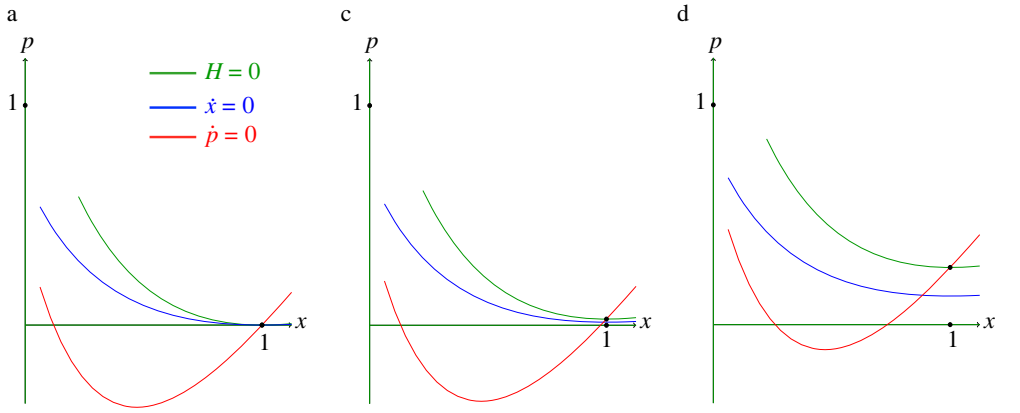

Figure 2. Plot of the relevant curves determining the dynamics of the Hill Hamiltonian system (3.3). On the one hand, the axes $x = 0$ and $p = 0$, which correspond, respectively, to extinction and to the one-dimensional deterministic model (3.2). On the other, the nullclines: $\dot{x} = 0$ (given by the curve $p = p_1(x)$, in blue colour, and the axis $x = 0$) and $\dot{p} = 0$ (given by the curve $p = p_2(x)$, in red, and the axis $p = 0$). Recall that the intersection of the nullclines gives rise to the equilibrium points of the system. Furthermore, they determine regions of growth/decrease of the corresponding variable, x or p. The 0-level curve of the Hamiltonian, $H = 0$, has been also plotted (in green its component $p = p_H(x)$, to which we must add the coordinate axes). The Hamiltonian character of system (3.3) makes $H = 0$, to form a kind of barrier for the solutions with initial conditions taken in $p > 0$, $x > 0$ and $H(x, p) < 0$. All three plots follow the same labels as in figure 1: (a) $\varphi = 10^{-5}$, (c) $\varphi = 10^{-2}$ and (d) $\varphi = 10^{-1}$. For a qualitative sketch of the dynamics in the Hamiltonian phase space and the bottleneck region responsible for the long transients, see figure 3.

— The solution of $H(x, p) = 0$, which is constituted by three curves: $x = 0$, $p = 0$ and $p = p_H(x)$, where

$$p_H(x) := \log\left(\frac{\epsilon + x^2}{x}\right),$$

has a global minimum at $x_{\min,\,\mathrm{H}} = \sqrt{\epsilon}$, with $p_{\min,\,\mathrm{H}} = p_H(x_{\min,\,\mathrm{H}}) = \log(2\sqrt{\epsilon})$. The value of ϵ for which $p = p_H(x)$ reaches its minimum on $p = 0$ is $\epsilon = \epsilon_c = 1/4$, and the point is $x_{\min,\,\mathrm{H}} = x_{\mathrm{crit}} = 1/2$.

— The x-nullcline, $\dot{x} = 0$, which has two branches: $x = 0$ and $p = p_1(x)$, where

$$p_1(x) := \frac{1}{2}\log\left(\frac{x^2 + \epsilon}{x}\right) = \frac{1}{2}p_H(x).$$

— The p-nullcline, $\dot{p} = 0$, formed by $p = 0$ and $p = p_2(x)$, where

$$p_2(x) := \log\left(\frac{3x^2 + \epsilon}{2x}\right),$$

which has a global minimum at $x_{\min,\,\mathrm{p}} = \sqrt{\epsilon/3}$, with $p_{\min,\,\mathrm{p}} = p_2(x_{\min,\,\mathrm{p}}) = \log\sqrt{3\epsilon}$. Moreover, $p = p_2(x)$ is tangent to $p = 0$ for $\epsilon = \epsilon_{\mathrm{end}} = 1/3$. For $\epsilon > \epsilon_{\mathrm{end}}$, one has $p_2(x) > 0$.

The aim of this Hamiltonian approach is to recover the qualitative behaviour for the extinction times shown by GS (see the upper panel in figure 1) and provide a theoretical tool to make useful predictions of transient times semi-analytically. To do so, we will compute the flight times of orbits starting at the bottleneck (see figure 3*a*) just after the s-n bifurcation takes place: $\epsilon = \epsilon_c$ or, equivalently, $\varphi = \epsilon - \epsilon_c = 0$. These flight or transient times provide a qualitatively good approximation for the extinction times given by GS. They have been numerically computed for the Hill model, but similar results are obtained for the autocatalytic case. The values of p considered will be close to the deterministic model, i.e., $p = 0$. These numerics have been

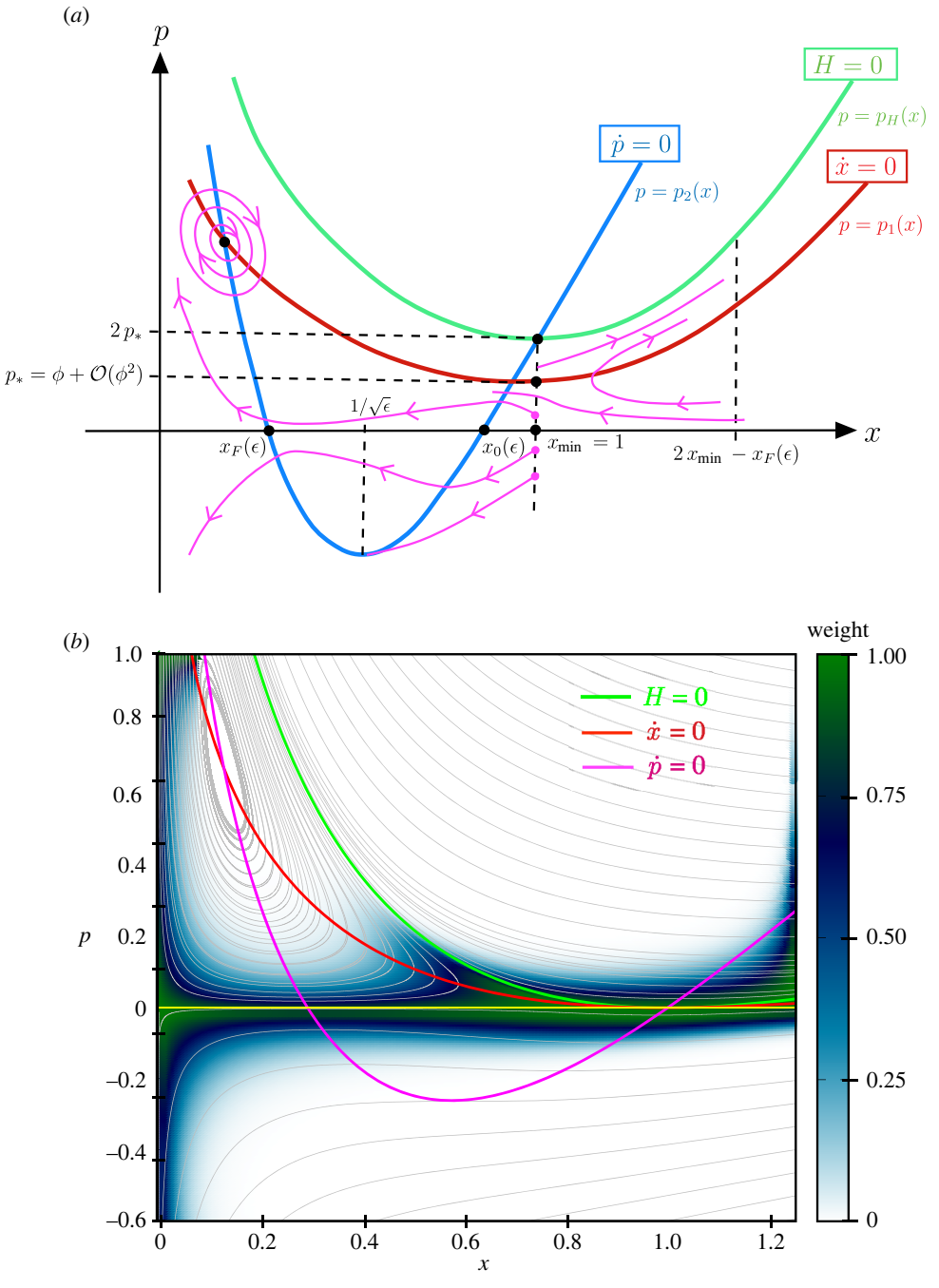

Figure 3. (*a*) Sketch of the dynamics for the Hill system given by equation (3.3). The Hamiltonian dynamics is ruled by the configuration of the curves $H = 0$ (green), the nullclines $\dot{x} = 0$ (red), $\dot{p} = 0$ (blue), and the invariant line $p = 0$ within the phase space. The intersections of the two nullclines give rise to two equilibria: a saddle point, close to $(x_{\min}, p_*)$, and a centre placed on the left-hand side of the region. The homoclinic connection to the saddle point around the elliptic one divides the zone close to the bottleneck in two regions: one where the flow goes leftwards (behind the homoclinic connection); and the other (above) where the flow goes rightwards. Some orbits (in violet) exhibiting different behaviours have been depicted. (*b*) Plot of the phase space of system (3.3) for $\varphi = 10^{-5}$. For each point in the grid, we compute the orbit having that as initial condition, calculating the approximate value of the action S on this orbit until it leaves the rectangle $[0, 1.22] \times [-0.8, 1]$ and its corresponding probability (or weight), $e^{-S\Omega}$. Darker coloured regions relate to orbits with (approximately) higher probability. The curves $H = 0$ (green light), the nullclines $\dot{x} = 0$ (red), $\dot{p} = 0$ (magenta), and some orbits (grey) are also shown.

performed in the following way (take the sketch in figure 3*a* as a reference): fixed the value of ϵ, let $p_{\text{bottom}}(\epsilon) < 0$ be the value of p such that the orbit with i.c. $(x(0), p(0)) = (1., p_{\text{bottom}})$ intersects tangentially the curve $p = p_2(x)$ (one of the connected components of $\dot{p} = 0$) at its minimum; take around 200, for instance, equidistributed initial conditions $(1, p_0)$, with $p_{\text{bottom}} < p_0 < |p_{\text{bottom}}|$, and compute numerically the corresponding orbit until it reaches the line $x = 0.25\, x_F(\epsilon)$ (if the flow goes leftwards) or the line $x = 2 - 0.25\, x_F(\epsilon)$ (if the flow goes rightwards). This defines a time that we denote by $T(p_0)$ or, for a generic p_0 in this segment, by $T(\epsilon)$. The point $(x_F(\epsilon), 0)$ is the smallest of the two points in which the p-nullcline $p = p_2(x)$ intersects $p = 0$, see figure 3*a*. The line $x = 1$ stands at the same x-distance of $x = 2 - 0.25 x_F(\epsilon)$ as $x = 0.25\, x_F(\epsilon)$. There is no significant change in T if one considers lines closer to the axis $x = 0$. The direction taken by the orbit (leftwards or rightwards) is determined by the location of the initial condition $(1, p_0)$ with respect to the homoclinic connection to the saddle point, near the bottleneck. This homoclinic connection contains in its interior an elliptic equilibrium point (figure 3*a*).

Interestingly, close to the bifurcation (i.e. $\varphi \gtrsim 0$), the behaviour of the flight time depends on the initial condition for the momentum variable $p(0) = p_0$ but not on x_0. If $p_0 > \varphi + \mathcal{O}(\varphi^2)$ the extinction time follows the deterministic scaling law $T \sim \varphi^{-1/2}$ (results not shown). By contrast, orbits with $p_0 < \varphi + \mathcal{O}(\varphi^2)$ exhibit a scaling function whose shape is essentially the same as the one obtained by GS. Such differences in behaviour appear to be governed by the geometry of the phase space (x, p) shown in figure 2. When $\varphi \to 0$ and $p_0 < \varphi + \mathcal{O}(\varphi^2)$, the orbits cross the region of the phase space contained within the nullcline $\dot{p} = 0$ (precisely, $p = p_2(x)$, depicted in blue in figure 3*a*) and the horizontal lines $p \simeq \varphi + \mathcal{O}(\varphi^2)$ and $p = 0$ (depending on the sign of p_0). This sojourn alters the properties of the slowing down, thus changing the scaling behaviour of the flight time. An analytic proof of that has been deferred to §a. That is, a similar behaviour to the scaling function $\mathcal{G}$ is obtained under both approaches, GS and Hamiltonian, close to the bifurcation. The flat scaling law for the extinction times (which do not depend on Ω when changing φ, displayed in figure 1) matches the GS running close to the bifurcation threshold (red rectangle), for $\Omega = 10^3$. Note also that the flat shape close to this threshold starts bending at $\varphi \approx 5 \times 10^{-4}$ (for this system size). Different system sizes also drive to good matching between GS results and the (Hamiltonian) transient times. For instance, system sizes ranging from $\Omega = 500$ to $\Omega = 8 \times 10^3$ show bending values of the flat region within the range $\varphi \in [3 \times 10^{-4}, 8 \times 10^{-4}]$ (results not shown; see also [28] to see this effect with GS).

Last, but not least, in order to shed some light onto the picture described above, we have quantified the importance of different sets of orbits of the Hamiltonian system (2.6). According to the path integral representation of a stochastic process, the weight (probability) of each trajectory is determined by their associated action S (see equation (2.5)). The rationale for this quantification goes as follows. Consider equation (2.5), which provides the path integral representation of the propagator, i.e. the conditional probability of a transition between state x_i at time t_i to state x_f at time t_f (e.g. Kubo *et al*. [31]). Concerning this representation, the propagator can be written as a weighted sum over all the possible sample paths connecting the initial and final states. The weight associated with each sample path is given by the exponential of minus the corresponding action, S, times the system size, Ω. Furthermore, given the form of equation (2.5) and that $\Omega \gg 1$, we can estimate the propagator using asymptotic arguments (such as the Laplace method or the saddle point approximation [42]). As we are working in a regime where $\Omega \gg 1$, the main contribution to the sum comes from the path that maximizes the action. Since the weight of all other trajectories is exponentially suppressed and, asymptotically, their contributions are negligible, the propagator is proportional to the weight of the path such that $\delta S = 0$. This path is the solution of the Hamilton equations (2.6). These arguments allow us to identify the exponential weight of the corresponding Hamiltonian trajectory as an estimator of their statistical weight.

In order to estimate approximate values for such weights, we have considered a grid $(x_0, p_0) \in [0, 1.22] \times [-0.8, 1]$ of initial conditions and computed numerically their orbits until they leave the rectangle. Let us denote by $\Gamma_0 = \Gamma(x_0, p_0)$ the piece of orbit with initial conditions (x_0, p_0) and escaping time $\tau(x_0, p_0)$. We have calculated the estimate value of the action S along Γ_0

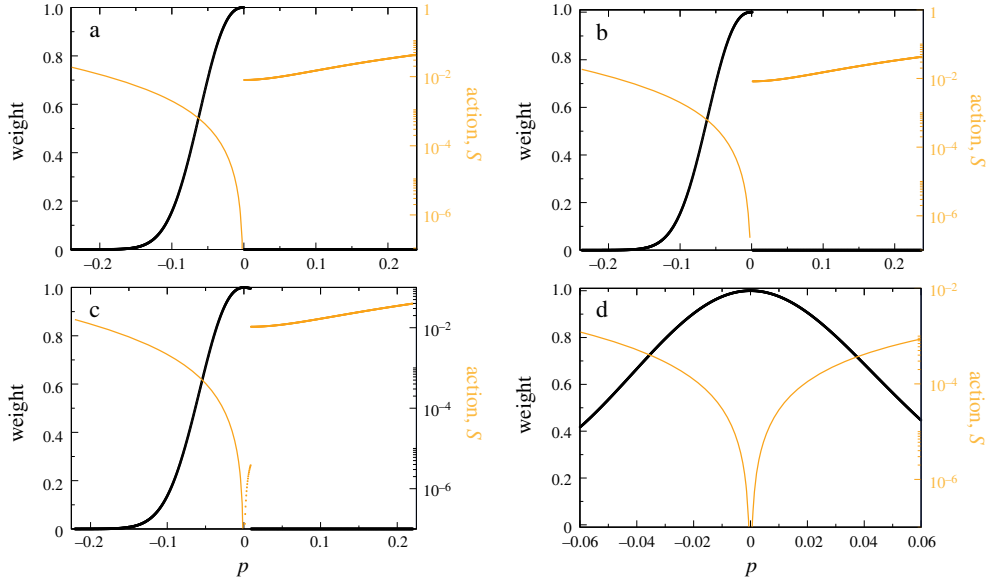

Figure 4. Weight of the regions in p along which stochastic realizations will pass (black lines) for the Hill model, and the associated action (orange dots) computed from the initial conditions $x(0) = 1$ and $p(0) \equiv p$. The four panels show the system's behaviour for the same labels indicated in figure 1, given by (a) $\varphi = 10^{-5}$, (b) $\varphi = 10^{-3}$, (c) $\varphi = 10^{-2}$ and (d) $\varphi = 10^{-1}$.

by approximating its line integral by the sum over the (discrete) numerically computed orbit. Precisely, if Γ_0 is approximated by the set of points $\{(x(t_k), p(t_k)) \mid k = 0 \div N\}$ then

$$S(\Gamma_0) = \int_0^{\tau(x_0,p_0)} p\dot{x} - H(x,p)\,\mathrm{d}t$$
$$\simeq \sum_{k=1}^{N} (p(t_k)\dot{x}(t_k) - H(x(t_k), p(t_k))) \cdot \sqrt{\dot{x}(t_k)^2 + \dot{p}(t_k)^2} \cdot (t_k - t_{k-1}).$$

The results are displayed in figure 3*b*. The colour of each point (x_0, p_0) denotes the weight of its orbit Γ_0, being the green-dark blue regions those with maximum weights (lowest action). Moreover, a similar computation has been done for those orbits starting at (x_0, p_0) with $x_0 = 1$ and $p_{\text{bottom}} < p_0 < |p_{\text{bottom}}|$. The orange data in figure 4 correspond to $(p_0, S(\Gamma(p_0)))$. In black colour, their corresponding weight (probability) (2.5). Figure 4 shows that, near the bifurcation, the only statistically significant trajectories (i.e. those trajectories with lower actions) are those with initial condition $p_0 < \varphi + \mathcal{O}(\varphi^2)$, as shown in figure 4*a*,*b*. These paths are the ones that contribute to the stochastic scaling function. By contrast, as we move away from the critical point, both orbits with positive and negative initial values of p become statistically significant, as depicted in figure 4*c*. Eventually (figure 4*d*), trajectories with both positive and negative p_0 have similar weights and, therefore, the behaviour of the system becomes a mixture of both characteristic behaviours.

(a) On the scaling law for $T(\epsilon)$

Let us focus here on the autocatalytic model. A similar approach can be performed for the Hill equation. We follow the procedure introduced in [12], where Residue Theorem is applied in a convenient way for a one-dimensional system. We will see that a similar argument can be extended to our case, with two variables x and p. From the first equation in system (3.4),

$$\dot{x} = x^2 e^p - (x^3 + \epsilon x)e^{-p} =: \tilde{f}(x, p, \epsilon),$$

it follows that the time $T(\epsilon)$ invested by a solution with initial condition on $x = x_{\text{ini}}$ to reach $x = x_{\text{end}}$ is given by

$$T(\epsilon) = \int_{x_{\text{ini}}}^{x_{\text{end}}} \frac{1}{\tilde{f}(x, p, \epsilon)}\, \mathrm{d}x. \tag{3.5}$$

Without loss of generality, we can assume that this interval is symmetric with respect to $x_{\min}$, the x-value where the s-n bifurcation occurs for $p = 0$.

Proposition 3.1. *Let $T(\epsilon)$ be the flight time spent by a solution of system (3.4) with initial condition on $x = x_{ini}$ to reach $x = x_{end}$, defined by equation (3.5). Then, there exists constants $p_- = \mathcal{O}(1) < -1/4$ and $p_+ = \varphi + \mathcal{O}(\varphi^2) > 0$, such that:*

— *If $p > p_+$ then $T(\varphi)$ behaves, in logarithmic scale, as*

$$\log T(\varphi) \sim -\frac{1}{2} \log \varphi.$$

That is, it satisfies the expected scaling law for a s-n bifurcation in a deterministic system.

— *If $p_- < p < p_+$, there exists a constant $\tilde{C} > 1$, independent of φ, such that*

$$T(\varphi) \geq \tilde{C} + \mathcal{O}(\varphi). \tag{3.6}$$

In logarithmic scale this corresponds to $\log T(\varphi) \geq \log(\tilde{C} + \mathcal{O}(\varphi))$.

The aim of this Proposition is to compute the first-order approximation of $T(\epsilon)$ in terms of $\varphi = \epsilon - \epsilon_c$. To do it, note first that

$$x^2 \mathrm{e}^p - (x^3 + \epsilon x)\mathrm{e}^{-p} = -x\mathrm{e}^{-p}(x^2 - \mathrm{e}^{2p}x + \epsilon) = \left(x - \frac{1}{2}\right)^2 + (1 - \mathrm{e}^{2p})x + \varphi,$$

where in this case $\varphi = \epsilon - (1/4)$, being $\epsilon_c = 1/4$ the value of ϵ at which the system undergoes the s-n bifurcation. Recall that the corresponding x-value for $\epsilon = \epsilon_c$ is $x_{\min} = x_c = 1/2$. If we apply the change of variables $y = x - (1/2)$ then $y(t)$ satisfies the following ODE:

$$\dot{y} = -\mathrm{e}^{-p}\left(y + \frac{1}{2}\right)\left(y^2 + (1 - \mathrm{e}^{2p})\left(y + \frac{1}{2}\right) + \varphi\right) =: f(y, p, \varphi). \tag{3.7}$$

In particular,

$$f(0,0,0) = 0 \quad \text{and} \quad \frac{\partial f}{\partial \varphi}(y, p, \varphi) = -\mathrm{e}^{-p}\left(y + \frac{1}{2}\right) \Rightarrow \frac{\partial f}{\partial \varphi}(0,0,0) = -\frac{1}{2} \neq 0. \tag{3.8}$$

So, therefore, we introduce the following lemma.

Lemma 3.2. *There exists an open set $\mathcal{U} \in \mathbb{R}^2$, containing $(0,0)$, and a $\mathcal{C}^\infty$-function*

$$\begin{array}{rccc} g: & \mathcal{U} & \longrightarrow & \mathbb{R} \\ & (y,p) & \longmapsto & \varphi = g(y,p) \end{array}$$

such that $g : \mathcal{U} \to g(\mathcal{U})$ is bijective and satisfies that $f(y, p, \varphi) = 0 \Leftrightarrow \varphi = g(y, p)\ \forall (y, p) \in \mathcal{U}$.

Let us denote, by commodity, $\varphi = \varphi(y, p) = g(y, p)$. Then, $\varphi(y, p)$ admits the following Taylor expansion around $(0,0)$:

$$\varphi(y, p) = p - y^2 + 2py + p^2 + \mathcal{O}_3(y, p), \tag{3.9}$$

where $\mathcal{O}_3(y, p)$ stands for terms of order at least 3 in y and p.

Proof. Proof (of lemma 3.2) Conditions (3.8) allow us to apply the Implicit Function Theorem and prove the first assertion of the lemma. Regarding the second one, we seek for

$$\varphi(y,p)=\varphi(0,0)+\frac{\partial\varphi}{\partial y}(0,0)\,y+\frac{\partial\varphi}{\partial p}(0,0)\,p + \frac{1}{2}\left(\frac{\partial^2\varphi}{\partial y^2}(0,0)\,y^2+2\frac{\partial^2\varphi}{\partial y\partial p}(0,0)\,yp+\frac{\partial^2\varphi}{\partial p^2}(0,0)\,p^2\right)+\mathcal{O}_3(y,p). \tag{3.10}$$

Standard recurrent differentiation of equation $f(y,p,\varphi)=0$ - with respect to y and p - and substitution onto $y=p=0$ gives $\varphi_y(0,0)=0$, $\varphi_p(0,0)=0$, $\varphi_{yp}(0,0)=2$, $\varphi_{yy}(0,0)=-2$, and $\varphi_{pp}(0,0)=2$. This leads to expression (3.9). ■

From $\varphi=p-y^2+2py+p^2+\mathcal{O}_3(y,p)$, it follows that $0=y^2-2py-p^2-p+\varphi+\mathcal{O}(\varphi^3)\Rightarrow(y-p)^2=2p^2+p-\varphi+\mathcal{O}(\varphi^3)$ and so (using the Taylor expansion for $\sqrt{1+x}$ with $|x|<1$),

$$f(y,p,\varphi)=0\Leftrightarrow y=y_\pm=p\pm\sqrt{2p^2+p-\varphi}+\mathcal{O}(\varphi^3).$$

Note that for $p=0$ and $\varphi>0$, one has[1] $y_\pm=\pm\mathrm{i}\sqrt{\varphi}+\mathcal{O}(\varphi)$. Hence, for $p\sim 0$, we have that $y_\pm$ are close to $y_\pm^0=\pm\mathrm{i}\sqrt{\varphi}$. Since our system undergoes a s-n bifurcation at $p=0$, $\varphi=0$, we focus our attention in the case where $2p^2+p-\varphi$ is negative, which moves the new equilibrium points $y_\pm\sim y_\pm^0$ to the complex plane. This polynomial factorizes as $2p^2+p-\varphi=2(p-p_-)(p-p_+)$, where

$$p_\pm=\frac{-1\pm\sqrt{1+8\varphi}}{4}\in\mathbb{R}\quad(\text{since }\varphi>0).$$

Indeed, $p_-<-(1/4)$ and

$$\begin{aligned}p_+&=\frac{-1+\sqrt{1+8\varphi}}{4}=\frac{-1+\sqrt{1+8\varphi}}{4}\cdot\frac{1+\sqrt{1+8\varphi}}{1+\sqrt{1+8\varphi}}=\frac{2\varphi}{1+\sqrt{1+8\varphi}}\\&=\frac{2\varphi}{1+(1-4\varphi+\mathcal{O}(\varphi^2))}=\frac{\varphi}{1-2\varphi+\mathcal{O}(\varphi^2)}\\&=\varphi(1+2\varphi+\mathcal{O}(\varphi^2))=\varphi+\mathcal{O}(\varphi^2).\end{aligned}$$

Roughly speaking, $p_-=\mathcal{O}(1)$ and $p_+=\mathcal{O}(\varphi)>0$. This factorization determines two cases to study: on the one hand, (i) $p>p_+$, where we have

$$y_\pm=p\pm\sqrt{2}\,\mathrm{i}\sqrt{(p-p_-)(p-p_+)}+\mathcal{O}(\varphi^3),$$

and, on the other, (ii) $p_-<p<p_+$, in which

$$y_\pm=p\pm\sqrt{2}\,\mathrm{i}\sqrt{(p-p_-)(p_+-p)}+\mathcal{O}(\varphi^3).$$

We are always assuming $|p|$ small. Note also that $\Im y_+>0$ and $\Im y_-<0$. It is worth mentioning that the value $p_+=\varphi+\mathcal{O}(\varphi^2)$ corresponds approximately to the value p_* appearing in the left-hand side of the phase space figure 3*a* (for the analogue Hill model). Here, p_* determines when the orbit starting at the initial point with $x=x_{\min}$ moves to the left or to the right. In other words, to start behind or above (respectively) the homoclinic connection to the hyperbolic equilibrium point, which exists close to $(x_{\min},p_+)$, around the elliptic equilibrium point on the left-hand side of figure 3*a*. We discuss the cases (i) $p>p_+$ and (ii) $p_-<p<p_+$ separately.

(i) Case $p>p_+$

As mentioned above, in this case, the orbit is located above the homoclinic connection and the flow goes rightwards. Let us take $\varphi_0\in(0,(1/12)]$, where $1/12=\epsilon_{\text{end}}-\epsilon_{\text{c}}=1/3-(1/4)$, the φ-interval for which the curve $\dot p=0$ intersects the line $p=0$. Now fix $\varphi\in(0,\varphi_0]$. From the change

[1]Sometimes, to emphasize its dependence on φ we will write $y_\pm(\varphi)$.

of variables $y = x - (1/2)$ and having in mind that our system is autonomous, the flight time $T(\varphi)$ of trajectories starting at $y = -\delta$ and reaching $y = \delta$ can be computed as

$$T_+(\varphi) = \int_{-\delta}^{\delta} \frac{1}{f(y,p,\varphi)}\,\mathrm{d}y, \tag{3.11}$$

for some $\delta > 0$ small. Let us consider $0 < \nu < p_+(\varphi_0)$, independent of φ, such that for $(y,p) \in W = [-\delta,\delta] \times (0,\mathrm{i}\nu]$ the function $f(y,p,\varphi)$ does not vanish, except at the point $y = y_+(\varphi) \simeq \mathrm{i}\sqrt{\varphi}$. In other words, $1/f$ is meromorphic in W and has a unique pole $y_+ \in W$. Furthermore, this pole is simple. Let us denote by $\gamma = \partial^+ W$ the (positively oriented) border of W. Thus, $\gamma = \gamma_1 \cup \gamma_2 \cup \gamma_3 \cup \gamma_4$, being γ_1 the segment placed on $p = 0$, γ_2 the one on $y = \delta$, γ_3 the one on $p = \mathrm{i}\nu$ and γ_4 the one on $y = -\delta$. Thus,

$$T_+(\varphi) = \int_{\gamma_1} \frac{1}{f(y,p,\varphi)}\,\mathrm{d}y = \int_{\gamma} \frac{1}{f(y,p,\varphi)}\,\mathrm{d}y + \sum_{j=2}^{4} \int_{\gamma_j} \frac{1}{f(y,p,\varphi)}\,\mathrm{d}y. \tag{3.12}$$

By the Residue Theorem, we have that

$$\int_{\gamma} \frac{1}{f(y,p,\varphi)}\,\mathrm{d}y = 2\pi\mathrm{i}\,\mathrm{Res}\left(\frac{1}{f}, y = y_+\right) = 2\pi\mathrm{i}\lim_{y\to y_+} \frac{y - y_+}{f(y,p,\varphi)} = \frac{2\pi\mathrm{i}}{\frac{\partial f}{\partial y}(y_+,p,\varphi)}. \tag{3.13}$$

Note that

$$y_+ = p + \sqrt{2}\,\mathrm{i}\sqrt{(p-p_-)(p-p_+)} + \mathcal{O}(\varphi^3) = \sqrt{2}\,\mathrm{i}c_1\sqrt{\varphi} + \mathcal{O}(\varphi^3),$$

since $p_+ = \mathcal{O}(\varphi)$, $p = \mathcal{O}(\varphi)$, $\sqrt{p-p_+} = \mathcal{O}(\sqrt{\varphi})$ and $\sqrt{p-p_-} = c_1 = \mathcal{O}(1)$. Substituting the expression $y_+ = \sqrt{2}\,\mathrm{i}c_1\sqrt{\varphi} + \mathcal{O}(\varphi)$ into

$$\frac{\partial f}{\partial y}(y,p,\varphi) = -\mathrm{e}^{-p}\left(3y^2 + 2(1-\mathrm{e}^{2p})\left(y + \frac{1}{2}\right) + y + \varphi\right), \tag{3.14}$$

leads to

$$\frac{\partial f}{\partial y}(y_+,p,\varphi) = c_2\,\mathrm{i}\sqrt{\varphi} + \mathcal{O}(\varphi)$$

and so equation (3.13) becomes

$$\int_{\gamma} \frac{1}{f(y,p,\varphi)}\,\mathrm{d}y = \frac{1}{\frac{\partial f}{\partial y}(y_+,p,\varphi)} = \frac{2\pi\mathrm{i}}{c_2\mathrm{i}\sqrt{\varphi} + \mathcal{O}(\varphi)} = \frac{c_3}{\sqrt{\varphi}} + \mathcal{O}(\varphi), \tag{3.15}$$

with $c_3 > 0$ a constant. Let us now deal with the computation on the curves γ_2, γ_3 and γ_4. We start with γ_2, which can be parameterizated by $\gamma_2(\sigma) = \delta + \mathrm{i}\nu\sigma$ for $\sigma \in [0,1]$. Since $f(\gamma_2(\sigma),\varphi) = f(\gamma_2(\sigma),0) + \mathcal{O}(\varphi)$ and by the compactness of the interval $[0,1]$ it follows that

$$\frac{1}{f(\gamma_2(\sigma),\varphi)} = \frac{1}{f(\gamma_2(\sigma),0)} + \mathcal{O}(\varphi).$$

Therefore,

$$\int_{\gamma_2} \frac{1}{f(y,p,\varphi)}\,\mathrm{d}y = \int_0^1 \frac{1}{f(\gamma_2(\sigma),\varphi)}\,\mathrm{d}\sigma = \int_0^1 \left(\frac{1}{f(\gamma_2(\sigma),0)} + \mathcal{O}(\varphi)\right)\mathrm{d}\sigma = c_4 + \mathcal{O}(\varphi), \tag{3.16}$$

c_4 being a constant. The same argument (and similar result) applies for the integrals over γ_3 and γ_4. In those cases, the parameterizations being $\gamma_3(\sigma) = (2\sigma - 1)\delta + \mathrm{i}\nu$ and $\gamma_4(\sigma) = -\delta + \mathrm{i}\nu(1-\sigma)$, with $\sigma \in [0,1]$, respectively. From these estimates and having in mind expressions (3.12) and (3.15), we obtain that

$$T_+(\varphi) = \frac{c_3}{\sqrt{\varphi}} + c_5 + \mathcal{O}(\varphi), \tag{3.17}$$

where c_3, c_5 are constants independent of φ. In logarithmic scale, this relation reads as

$$\log T_+(\varphi) \sim -\frac{1}{2}\log\varphi,$$

the expected scaling law for a s-n bifurcation in a one-dimensional deterministic system [12].

(ii) Case $p_- < p < p_+$

Contrary to what happened for $p > p_+$, now we are behind the homoclinic connection on the bottleneck and, therefore, the flow moves leftwards. Analogously to the case $p > p_+$, let us take $\varphi_0 \in (0, 1/12]$ and fix $\varphi \in (0, \varphi_0]$. To compute

$$T_-(\varphi) = \int_\delta^{-\delta} \frac{1}{f(y,p,\varphi)}\,\mathrm{d}y,$$

we consider $0 < \eta < 1/4$, independent of φ and $\eta = \mathcal{O}(1)$, such that $f(y,p,\varphi) \neq 0$ for any $(y,p) \in V = [-\delta,\delta] \times [-\mathrm{i}\eta, 0)$ except the point $y_-(\varphi)$, where it has a simple zero. As above, this means that $1/f$ is meromorphic in V and has a unique pole (simple) at $y = y_-(\varphi) \in V$. We follow the same argument as in the previous case: define $\Gamma = \Gamma_1 \cup \Gamma_2 \cup \Gamma_3 \Gamma_4$, the positively oriented border of V. Γ_1 is the segment on $p = 0$, Γ_2 the one on $y = -\delta$, Γ_3 the one on $p = -\mathrm{i}\eta$ and Γ_4 the one on $y = \delta$. Therefore,

$$T_-(\varphi) = -\int_{\Gamma_1} \frac{1}{f(y,p,\varphi)}\,\mathrm{d}y = -\int_{\Gamma} \frac{1}{f(y,p,\varphi)}\,\mathrm{d}y + \sum_{j=2}^{4} \int_{\Gamma_j} \frac{1}{f(y,p,\varphi)}\,\mathrm{d}y. \tag{3.18}$$

Like in the previous case, we compute the first line integral by the Residue Theorem:

$$\int_\Gamma \frac{1}{f(y,p,\varphi)}\,\mathrm{d}y = 2\pi\mathrm{i}\,\mathrm{Res}\left(\frac{1}{f}, y = y_-\right) = 2\pi\mathrm{i} \lim_{y\to y_-} \frac{y - y_-}{f(y,p,\varphi)} = \frac{2\pi\mathrm{i}}{\frac{\partial f}{\partial y}(y_-,p,\varphi)}. \tag{3.19}$$

To do it we need an estimate of $y_- = p - \sqrt{2}\,\mathrm{i}\sqrt{(p-p_-)(p_+-p)}$, for $p \in [-\mathrm{i}\eta, 0)$, in terms of φ. Remember that $p_+ = \mathcal{O}(\varphi)$ and $p_- = \mathcal{O}(1)$. Given a continuous function h, we denote by $g \geq \mathcal{O}(h(\varphi))$ to mean that there exists a constant d_1 such that $g \geq d_1 h(\varphi)$. Likely, we write $g \leq \mathcal{O}(h(\varphi))$ to express that $g \leq d_2 h(\varphi)$, for a suitable constant d_2. In our case, these bounds can be taken uniform due to the compactness of $\bar{V}$. Take any $(y,p) \in V$. On the one hand, we have that $p - p_- = \mathcal{O}(1) \Rightarrow \sqrt{p-p_-} = \mathcal{O}(1)$. Besides, it is also clear that $\mathcal{O}(\varphi) \leq p_+ - p \leq \mathcal{O}(1)$ and so $\mathcal{O}(\sqrt{\varphi}) \leq \sqrt{p_+ - p} \leq \mathcal{O}(1)$. Joining both estimates it turns out that

$$\mathcal{O}(\sqrt{\varphi}) \leq \sqrt{(p-p_-)(p_+-p)} \leq \mathcal{O}(1),$$

and, since $0 \leq |p| \leq \mathcal{O}(1)$,

$$\mathcal{O}(\sqrt{\varphi}) \leq p - \sqrt{2}\,\mathrm{i}\sqrt{(p-p_-)(p_+-p)} \leq \mathcal{O}(1).$$

That is $\mathcal{O}(\sqrt{\varphi}) \leq y_-(\varphi) \leq \mathcal{O}(1)$. We will use this bound to get an estimate for

$$\frac{\partial f}{\partial y}(y_-,p,\varphi) = -\mathrm{e}^{-p}\left(3y_-^2 + 2(1-\mathrm{e}^{2p})\left(y_- + \frac{1}{2}\right) + y_- + \varphi\right).$$

On one side, it is straightforward to check that e^{-p} and $y_- + (1/2)$ are $\mathcal{O}(1)$. Moreover,

$$\mathcal{O}(\varphi) \leq 3y_-^2 \leq \mathcal{O}(1), \quad 0 < 2(1-\mathrm{e}^{2p}) \leq \mathcal{O}(1).$$

All these bounds together to the one for y_- implies that

$$\mathcal{O}(\varphi) \leq -\mathrm{e}^{-p}\left(3y_-^2 + 2(1-\mathrm{e}^{2p})\left(y_- + \frac{1}{2}\right) + y_- + \varphi\right) \leq \mathcal{O}(1).$$

Consequently,

$$-\int_\Gamma \frac{1}{f(y,p,\varphi)}\,\mathrm{d}y = \frac{2\pi\mathrm{i}}{\frac{\partial f}{\partial y}(y_-,p,\varphi)} \geq \mathcal{O}(1).$$

That is, there exists a constant $c_5 > 1$ such that

$$-\int_\Gamma \frac{1}{f(y,p,\varphi)}\,\mathrm{d}y \geq c_5, \tag{3.20}$$

uniformly in V. The contribution of the integrals

$$\int_{\Gamma_j} \frac{1}{f(y,p,\varphi)}\,\mathrm{d}y, \quad j=2,3,4,$$

follow *mutatis mutandis* the same argument as employed in the case $p>0$. Namely, for any parameterization $\Gamma_j(\sigma)$ of the segments Γ_j[2] one can see that $f(\Gamma_j(\sigma),\varphi)=f(\Gamma_j(\sigma),0)+\mathcal{O}(\varphi)$. So, taking into account the compactness of the σ-interval $[0,1]$, it follows that

$$\int_{\Gamma_j} \frac{1}{f(y,p,\varphi)}\,\mathrm{d}y=\int_0^1 \frac{1}{f(\Gamma_j(\sigma),\varphi)}\,\mathrm{d}\sigma=\int_0^1\left(\frac{1}{f(\Gamma_j(\sigma),0)}+\mathcal{O}(\varphi)\right)\mathrm{d}\sigma=c_{4+j}+\mathcal{O}(\varphi), \tag{3.21}$$

for $j=2,3,4$. From expressions (3.21), (3.20) and (3.18), we derive the following estimate for the flight-time,

$$T_-(\varphi)\geq \tilde{C}+\mathcal{O}(\varphi). \tag{3.22}$$

$\tilde{C}>1$ a constant independent of φ. In logarithmic scale this corresponds to $\log T_-(\varphi)\geq \log(\tilde{C}+\mathcal{O}(\varphi))$.

4. Discussion

We have analysed the dynamical behaviour of two stochastic systems close to a tipping point given by a s-n bifurcation (first-order phase transition) using a Hamiltonian approach, mainly regarding the slowing down phenomena observed in the relaxation times towards their absorbing state. We recently explored the effect of intrinsic noise in simple models with cooperation undergoing s-n bifurcations including the autocatalytic replicator and two-species hypercycles [28]. Somewhat counterintuitively, we found that the deterministic ghosts were robust to noise. However, the scaling law of the mean extinction times was shown to follow a rather more complicated scaling function than its deterministic counterpart (see equation (1.1)). This more complex scaling law was only identified numerically using Gillespie simulations and was found to be general (independent of the system's size). Therefore, a theory able to explain these numerical results was still lacking. In an attempt to provide a general theory explaining and identifying the mechanisms underlying this change in behaviour identified by simulations, in particular concerning the origin of the scaling function, $\mathcal{G}(\cdot)$, we have reformulated the ME as a path integral. Hence, the solution of the ME is obtained as a weighted superposition of paths in the phase space of the Hamiltonian (2.4), which are given by the solutions of equations (2.6). Each such path is assigned a weight that depends exponentially on the action associated with it (see equation (2.5)) times the system size Ω.

The analyses of the paths and their weights yield a number of interesting results that shed some light onto the origin of both the robustness of the ghost behaviour in the presence of intrinsic noise and the scaling function $\mathcal{G}$. First, when the system is close to the bifurcation ($\varphi=\epsilon-\epsilon_c=\mathcal{O}(10^{-3})$ or smaller), there is a set of solutions (corresponding to $p(t=0)<\varphi+\mathcal{O}(\varphi^2)$) of the Hamiltonian system (equations (2.6)) that undergo very long transients when crossing the regions of the phase space shown in figure 2. Furthermore, as shown in figure 1 (lower panel), when we compute how the flight time associated with the paths varies as φ changes, we realize that, rather than following the deterministic scaling law $\varphi^{-1/2}$, it is qualitatively the same as the one computed numerically by means of the SSA for values of $\varphi\leq 10^{-3}$ (see figure 1, upper panel). By contrast, solutions of equations (2.6) with $p(t=0)>\varphi+\mathcal{O}(\varphi^2)$ exhibit the same scaling behaviour as the deterministic limit, i.e. flight time $\sim\varphi^{-1/2}$. Further insight is obtained from the quantification of the action and weight associated with each path, as shown in figure 4. These results show that, for $\varphi\leq 10^{-3}$, the only statistically significant paths are those corresponding to $p(t=0)<\varphi+\mathcal{O}(\varphi^2)$, whereas all the paths with $p(t=0)>\varphi+\mathcal{O}(\varphi^2)$ have negligible small weights. Taken together, these results suggest that, close to the bifurcation, the only statistically significant paths, and consequently the

[2]We named it with the same letter since there is no problem of misunderstanding.

only ones that will contribute to the observable behaviour, are those with $p(t=0) < \varphi + \mathcal{O}(\varphi^2)$, for which the flight time is $\simeq \mathcal{G}(\varphi)$.

Our core outcome is therefore that the qualitative behaviours displayed by the paths of the Hamiltonian equation (2.4), are thus mimicked by or translated to the observable behaviour of the stochastic system, provided that they are statistically significant. In the specific case of systems whose mean-field model exhibits a s-n bifurcation, the delayed relaxation and shape of the function $\mathcal{G}$ are the statistically significant features that are passed on to the stochastic system. This explains the robustness of the ghost behaviour to intrinsic noise and the scaling behaviour of the mean extinction times, $\bar{T}_e$ found numerically in [28]. It is noteworthy that, although we have illustrated our theory with two specific examples, the same properties should extend in a universal way to all stochastic systems whose associated Hamiltonian system exhibits the same behaviour.

Finally, we conclude that the analysis we have put forward here can have great relevance to analyse qualitative behaviours of complex stochastic systems, specifically, close to phase transitions or bifurcations, in a way that does not require a substantial computational effort. By analysing the orbits of the corresponding Hamiltonian system and the different qualitative behaviours it can sustain, we will be able to evaluate which behaviours are associated with statistically relevant orbits, and therefore should manifest themselves at the level of the observable behaviour of the stochastic system. Our approach thus provides a useful tool for predicting stochastic transients close to a tipping point.

Data accessibility. This article has no additional data.

Authors' contributions. J.T.L.: conceptualization, data curation, formal analysis, funding acquisition, investigation, methodology, software, supervision, visualization, writing—original draft; T.A.: conceptualization, data curation, formal analysis, funding acquisition, investigation, methodology, software, supervision, validation, visualization, writing—original draft; C.P.G.: conceptualization, data curation, formal analysis, funding acquisition, investigation, methodology, resources, software, supervision, validation, visualization, writing—original draft; J.S.: conceptualization, data curation, formal analysis, funding acquisition, investigation, methodology, software, supervision, validation, visualization, writing—original draft.

All authors gave final approval for publication and agreed to be held accountable for the work performed therein.

Conflict of interest declaration. We declare we have no competing interests.

Funding. T.A., J.S. and J.T.L. would like to thank the Laboratorio Subterráneo de Canfranc (LSC) for kind hospitality and strong support during the development of this research. This work has been funded by the Spanish State Research Agency (AEI), through the Severo Ochoa and Maria de Maeztu Program for Centers and Units of Excellence in R&D (CEX2020-001084-M). We thank CERCA Programme/Generalitat de Catalunya for institutional support. J.S. and T.A. have been funded by grants RTI2018-098322-B-I00 and PID2021-127896OB-I00 funded by MCIN/AEI/10.13039/501100011033 'ERDF A way of making Europe'. J.S. has been also funded by the Ramón y Cajal contract (RYC-2017-22243) funded by MCIN/AEI/10.13039/501100011033 'FSE invests in your future'. J.T.L. has been funded by the Spanish project PGC2018-098676-B-100 funded by MCIN/AEI/10.13039/501100011033 'ERDF A way of making Europe'; by the Spanish project PID2021-122954NB-I00 funded by MCIN/AEI/10.13039/501100011033/ and 'ERDF A way of making Europe'; and by a grant from the 'Ayudas para la recualificación del sistema universitario español para 2021-2023'. J.T.L. also thanks the hospitality of LSC as a hosting institution of this grant.

References

1. Goldenfeld N. 1992 *Lectures on phase transitions and the renormalization group*. Boca Raton, FL: CRC Press.
2. Kuznetsov Y. 1998 *Elements of applied bifurcation theory*, 2nd edn. New York, NY: Springer.
3. Strogatz SH. 2000 *Nonlinear dynamics and chaos with applications to physics, biology, chemistry, and engineering*. Boulder, CO: Westview Press.
4. Hohenber PC, Halperin BI. 1977 The theory of dynamic critical phenomena. *Rev. Mod. Phys.* **49**, 435–479. (doi:10.1103/RevModPhys.49.435)
5. Strogatz SH, Westervelt RM. 1989 Predicted power laws for delayed switching of charge density waves. *Phys. Rev. B* **40**, 10 501–10 508. (doi:10.1103/PhysRevB.40.10501)

6. Suzuki M, Kaneko K, Takesue S. 1982 Critical slowing down in stochastic processes I. *Progr. Theor. Phys.* **67**, 1756–1775. (doi:10.1143/PTP.67.1756)
7. Suzuki M, Takesue S, Sasagawa F. 1982 Critical slowing down in stochastic processes II. *Progr. Theor. Phys.* **68**, 98–115. (doi:10.1143/PTP.68.98)
8. Hastings A, Abbott K, Cuddington K, Francis T, Gellner G, Lai Y-C, Morozov A, Petrovskii S, Scranton K, Zeeman MJ. 2018 Transient phenomena in ecology. *Science* **361**, eaat6412. (doi:10.1126/science.aat6412)
9. Vidiella B, Fontich E, Valverde S, Sardanyés J. 2021 Habitat loss causes long extinction transients in small trophic chains. *Theor. Ecol.* **14**, 641–661. (doi:10.1007/s12080-021-00509-7)
10. Sardanyés J, Pinero J, Solé R. 2019 Habitat loss-induced tipping points in metapopulations with facilitation. *Pop. Ecol.* **61**, 436–449. (doi:10.1002/1438-390X.12020)
11. Gimeno J. 2018 On the effect of time lags on a saddle-node remnant in hyperbolic replicators. *J. Phys. A: Math. Theor.* **51**, 385601. (doi:10.1088/1751-8121/aad02f)
12. Fontich E, Sardanyés J. 2008 General scaling law in the saddle-node bifurcation: a complex phase space study. *J. Phys. A: Math. Theor.* **41**, 468–482. (doi:10.1088/1751-8113/41/1/015102)
13. Sardanyés J, Solé R. 2006 Bifurcations and phase transitions in spatially-extended two-member hypercycles. *J. Theor. Biol.* **234**, 468–482. (doi:10.1016/j.jtbi.2006.07.014)
14. Canela J, Fagella N, Alsedà L, Sardanyés J. 2022 Dynamical mechanism behind ghosts unveiled in a map complexification. *Chaos, Solitons & Fractals* **156**, 111780. (doi:10.1016/j.chaos.2021.111780)
15. Vidiella B, Sardanyés J, Solé R. 2018 Exploiting delayed transitions to sustain semiarid ecosystems after catastrophic shifts. *J. R. Soc. Interface* **15**, 20180083. (doi:10.1098/rsif.2018.0083)
16. Sardanyés J, Solé R. 2007 The role of cooperation and parasites in non-linear replicator delayed extinctions. *Chaos, Solitons Fractals* **31**, 1279–1296. (doi:10.1016/j.chaos.2006.05.020)
17. Dugatkin LA. 2002 Animal cooperation among unrelated individuals. *Naturwiss.* **89**, 533–541. (doi:10.1007/s00114-002-0379-y)
18. Cassill DL, Butler J, Vinson SB, Wheeler DE. 2005 Cooperation during prey digestion between workers and larvae in the ant, *Pheidole padonia*. *Insect. Soc.* **52**, 339–343. (doi:10.1007/s00040-005-0817-x)
19. Ruppert EE, Fox RS, Barnes RD. 2004 *Invertebrate Zoology: A Functional Evolutionary Approach* (7th edn), pp. 112–148. USA: Brooks/Cole, Thomson Learning.
20. Chen MK, Hauser M. 2005 Modeling reciprocation and cooperation in primates: evidence for a punishing strategy. *J. Theor. Biol.* **235**, 5–12. (doi:10.1016/j.jtbi.2004.12.015)
21. Dai L, Vorselen D, Korolev KS, Gore J. 2012 Generic indicators of loss of resilience before a tipping point leading to population collapse. *Science* **336**, 1175–1177. (doi:10.1126/science.1219805)
22. Ungefroren H. 2021 Autocrine TGF-β in cancer: review of the literature and caveats in experimental analysis. *Int. J. Mol. Sci.* **22**, 977. (doi:10.3390/ijms22020977)
23. Duarte J, Januário C, Martins N, Sardanyés J. 2012 Scaling law in saddle-node bifurcations for one-dimensional maps: a complex variable approach. *Nonlin. Dyn.* **67**, 541–547. (doi:10.1007/s11071-011-0004-8)
24. Trickey ST, Virgin LN. 1998 Bottlenecking phenomenon near a saddle-node remnant in a Duffing oscillator. *Phys. Lett. A* **248**, 185–190. (doi:10.1016/S0375-9601(98)00665-3)
25. Kuehn C. 2008 Scaling of saddle-node bifurcations: degeneracies and rapid quantitative changes. *J. Phys. A: Math. Theor.* **42**, 045101. (doi:10.1088/1751-8113/42/4/045101)
26. Sardanyés J. 2008 Error threshold ghosts in a simple hypercycle with error prone self-replication. *Chaos, Solitons Fractals* **35**, 313–319. (doi:10.1142/S0218127410026460)
27. Sardanyés J, Fontich E. 2010 On the metapopulation dynamics of autocatalysis: extinction transients related to ghosts. *Int. J. Bifurcat. Chaos* **20**, 1–8. (doi:10.1142/S0218127410026460)
28. Sardanyés J, Raich C, Alarcón T. 2020 Noise-induced stabilization of saddle-node ghosts. *New J. Phys.* **22**, 093064. (doi:10.1088/1367-2630/abb549)
29. Sakurai JJ, Napolitano J. 2011 *Modern quantum mechanics*, 2nd edn. San Francisco, CA: Addison-Wesley.
30. Elgart V, Kamenev A. 2004 Rare event statistics in reaction-diffusion systems. *Phys. Rev. E* **70**, 041106. (doi:10.1103/PhysRevE.70.041106)
31. Kubo R, Matsuo K, Kitahara K. 1973 Fluctuation and relaxation of macrovariables. *J. Stat. Phys.* **9**, 51–96. (doi:10.1007/BF01016797)

32. Bressloff PC. 2014 *Stochastic processes in cell biology*. Springer: Berlin, Germany
33. Assaf M, Meerson B. 2006 Spectral theory of metastability and extinction in birth-death systems. *Phys. Rev. E* **97**, 200602. (doi:10.1103/PhysRevLett.97.200602)
34. Assaf M, Meerson B. 2010 Extinction of metastable sto-chastic populations. *Phys. Rev. E* **81**, 021116. (doi:10.1103/PhysRevE.81.021116)
35. Escudero C, Kamenev A. 2009 Switching rates of multistep reactions. *Phys. Rev. E* **79**, 041149. (doi:10.1103/PhysRevE.79.041149)
36. Gottesman O, Meerson B. 2012 Multiple extinction routes in stochastic population models. *Phys. Rev. E* **85**, 021140. (doi:10.1103/PhysRevE.85.021140)
37. Hinch R, Chapman SJ. 2005 Exponentially slow transitions on a Markov chain: the frequency of calcium sparks. *Eur. J. Appl. Math.* **16**, 427–446. (doi:10.1017/S0956792505006194)
38. Hill AV. 1910 The combinations of haemoglobin with oxygen and with carbon monoxide. *J. Physiol.* **40**, iv–vii.
39. Murray JD. 1992 *Asymptotic analysis*. New York, NY: Springer.
40. Gillespie DT. 1977 Exact stochastic simulation of coupled chemical reactions. *J. Phys. Chem.* **81**, 2340–2436. (doi:10.1021/j100540a008)
41. Lázaro JT, Sardanyés J, Alarcón T, Peña C. 2023 Dynamical systems and stochastic simulations software (autocatalytic replicator and Hill model). CORA. Repositori de Dades de Recerca. Version V1. (doi:10.34810/data691)
42. Gillespie DT. 2000 The chemical Langevin equation. *J. Chem. Phys.* **113**, 297–306. (doi:10.1063/1.481811)